Ultrafast electron injection kinetics and effect of plasmonic silver nanoparticle at organic dye-TiO$_2$ interface

Chinmoy Biswas[1], Md Soif Ahmed[1] and Sai Santosh Kumar Raavi[1,2]*

[1]Ultrafast Photo-physics and Photonics Laboratory, Department of Physics,

Indian Institute of Technology Hyderabad, Kandi-502 285, Telangana, India

[2]Department of Climate Change, Indian Institute of Technology Hyderabad, Kandi-502 285, Telangana, India

Dedicated to Professor D N Rao for his significant contributions and pioneering works in the
fields of spectroscopy, optics, nonlinear optics and photonics

In this mini review, we present the investigations on the electron injection kinetics of two thioalkyl substituted tetrathiafulvalene dye molecules in mesoporous TiO$_2$ layers for dye-sensitized solar cells (DSSCs). Steady-state absorption and photoluminescence (PL) spectroscopy techniques were employed to apprehend the excited state dynamics of the molecules as thin-film deposited on quartz and mesoporous TiO$_2$ layers. Time-resolved PL measurements at the "dye-TiO$_2$" interface provided initial evidence of electron injection by fast PL quenching decay dynamics for both the molecules. Detailed target analysis of the femtosecond transient absorption spectroscopy (TAS) data of the "dye-TiO$_2$" sample showed a multi-step ultrafast electron injection for both molecules where the fastest injection components were ≈374 fs and ≈314 fs for G1 and G3 molecules, respectively. Furthermore, the introduction of silver nanoparticles (AgNPs) at the dye-TiO$_2$ interface resulted in surface plasmon resonance induced ultrafast and enhanced electron-injection and reduced charge-recombination dynamics. We observed improved light trapping and hot electron injection from Ag NPs to TiO$_2$. © Anita Publications. All rights reserved.

Keywords: Plasmons, dye-sensitized solar cells, electron injection dynamics, ultrafast spectroscopy, silver nanoparticles.

1 Introduction

In the class of third generation solar cells or "emerging photovoltaics", Dye Sensitized Solar Cells (DSSCs) is among the most researched technology and have attracted significant research efforts over the last decades with the promise to lower the cost of solar power conversion modules considering the advantages of inexpensive material constituents with solution-processible, scalable, and reproducible device fabrication [1]. Since their first report in the 1990s, ruthenium (II) based organometallic complexes have been the most used sensitizers, leading to excellent photovoltaic performance [2]. However, metallic centre substituted sensitizers are very expensive due to the rarity of the metal ions in the environment. This resulted in extensive search for metal-free organic dyes, with large diversity in molecular structure design, that can tune absorption and HOMO-LUMO properties in a controlled manner [3]. Organic dyes bearing electron donating (*D*) and electron accepting (*A*) fragments linked by π-conjugated bridges, called push-pull dyes, have been the subject of intensive research for DSSC application due to extent of intramolecular charge transfer (ICT) occurring in the *D-π-A* structure. A mesoporous wide band gap semiconducting oxide layer composed of nanometre-sized particles that allow electronic conduction to take place is another important component of DSSC. Attached to the surface of this mesoporous nanocrystalline oxide film there is a monolayer of

---

the sensitizer dye. Following photoexcitation of the dye's *D-π-A* structure ICT takes place in dye's excited state, whereby electron population is transferred from the donor to the acceptor through the π-conjugated linker and thereafter in the injection of electrons into the conduction band (CB) of the oxide, generating the oxidized dye molecules [4]. After electron injection, the ground state of the dye is subsequently restored by electron donation from electrolyte which is itself regenerated at the counter electrode by electron passed through the external circuit, completing the DSSC operation. There are two key kinetic competitions limiting the efficiency of charge separation and thereby device performance: electron injection versus excited state decay to ground state via radiative transitions and dye regeneration versus electron back recombination from CB with dye cations [4]. Therefore, the kinetics of interfacial charge transfer between molecular dyes and semiconductor nanoparticles has attracted research attentions, in this context of DSSC [2]. A considerable progress toward the improvement of device efficiency and stability can still be achieved through better understanding and optimization of the fundamental charge-transfer processes [5]. In general, the rate of different charge transfer and recombination processes depends on the energy levels at the interfaces, the materials used, their morphology, and preparation conditions as well as the chemical interactions between them [6].

Till date, the efficiency of DSSC had been limited at a maximum of around ~ 13.5% among all of its variants [7]. This, in part, is due to distinct light absorption (by the dye molecules) and electron transport (in the nanostructure TiO$_2$) process in DSSC, contrary to the single crystal solar cells, where both the light absorption and charge transport take place in the same material. Over the last few years, researchers have tested different dyes [8-10], quantum dots [11, 12], active layer materials of different morphologies [13,14], and novel electrolytes [15] to improve the photo collection efficiency and electron transport of DSSC. Among the most notable improvement made in the field of DSSC is through the incorporation of subwavelength metal nanoparticles (NPs) elevating light harvesting, giving rise to improved optical absorption, carrier generation, and overall power conversion efficiency [16-18].

Following photo excitation in metal NPs incident photons are coupled to conduction band electrons, giving rise to collective oscillations of the electrons defined as localized surface plasmon resonance (LSPR). By tuning the geometry, dimension, and composition, the LSPR of metal NPs can be manipulated to capture selective bands of solar light to supplement or complement the absorption by the sensitizers [19]. The presence of plasmonic metal NPs increases optical path length of incident light due to scattering, augmenting the absorption and therefore overall efficiency [19]. Further, experiments have indicated that the enhancement in certain DSSCs arises from near field plasmonic effects [20], as have been identified to be important in enhancing many molecular optical processes [21]. In general, plasmonic effects in the DSSC can be categorized in two parts [19]: (1) radiative effects, where LSPR relaxes and re-radiates light into the absorptive layer or in other words the NPs act as a secondary light source enhancing local electric fields [22,23], and (2) non-radiative effects, where LSPR relaxes and energy is subsequently transferred to nearby wide band gap semiconductor, increasing the current generation. Again, the radiative effects could give rise to electric fields in the NPs' "near field" or light scattering into the NPs, "far-field". This far-field scattered light can ultimately be reabsorbed by the sensitizer in DSSC, enabling enhanced light absorption [19]. Whereas, in the near-field enhancement in the immediate vicinity of the NPs electromagnetic fields get locally enhanced, therefore the NPs integrated with DSSC act as a nanosized light concentrators focusing incident light on the metal surface within a small mode volume [19]. In other words, in this case NPs act like a second light source increasing the photon flux and therefore overall photons absorbed by the solar cell. The non-radiative effects also play a significant role and facilitate coupling of below band gap energy into the semiconductor. Two different non-radiative effects may contribute to enhance carrier generation in DSSC: hot-electron transfer (HET), and plasmon resonant energy transfer (PRET). Both non-radiative energy transfer processes have been studied in photodetectors [24] and solar photocatalysis [25] but remain poorly understood in the case of DSSC.

The charge carrier dynamics in both, normal DSSC and plasmon enhanced DSSC is key parameter in understanding device performance and further improvement on device and material fabrication strategy. Recently, a significant amount of research was focused on different time-resolved optical spectroscopy experiments like steady state and time resolved fluorescence and ultrafast transient absorption spectroscopy of both normal DSSC and plasmon induced DSSC, which yielded a wealth of information on the electron injection and charge recombination dynamics. For normal DSSC the solar cell efficiencies using inorganic dyes have been superior compared to DSSC using organic dyes [26]. However, on the incorporation of *D-π-A* (push-pull) geometry in the structure of organic dye molecule, enhanced efficiencies ~ 10% have been observed [5, 27]. Despite several investigations of electron injection dynamics on organic dye-sensitized TiO_2 nanoparticles, measurements on the organic chromophores with push-pull geometry and TiO_2 nanoparticles are limited [28-30]. Ultrafast (<100 fs) electron transfer is reported for most of the organic dye-sensitized TiO_2 nanoparticles, while multiexponential and picosecond components of electron injection were observed for inorganic dye-sensitized TiO_2 nano-particles [31,32]. The slower electron injection components are not frequently observed in organic dye-sensitized TiO_2 due to strong electronic coupling of the dye's excited state with the electronic states in the conduction band of TiO_2 leading to ultrafast electron transfer [31,33]. Recent work on push-pull dye sensitized TiO_2 NPs has shown slow electron injection and ascribed it to the injection from an excited ICT state [34]. Importantly, it is observed that the multi-exponential electron injection occurs predominantly only for sensitizers with D-π-A structure [35].

Additionally, due to incorporation of metal NPs in the DSSC system, the improved charge carrier densities along with the mechanism of carrier generation, charge separation, transport, and recombination at different interfaces in DSSC can be identified and decoupled their individual effect on photo conversion efficiency using time-resolved spectroscopic technique including transient absorption spectroscopy (TAS) and time-resolved photoluminescence (TrPL) technique. Snaith and co-workers studied the effect of 15 nm Au-SiO$_2$ nanoparticles incorporated in DSSC sensitized with Z907 dye and observed an enhanced transient absorption signal in amplitude due to the presence of NPs [22]. They explained this effect due to higher molecular absorption coefficients of Au nanoparticles relative to the sensitizer enhancing the photo-bleaching signal of the dye. The authors measured the decay kinetics of the photobleaching band at 520 nm and obtained a lifetime of 5 ps, which correlated well with the known electron-phonon relaxation time of ~ 3 ps. They attributed this fast decay to the relaxation of the hot electron population and further suggested that plasmonic enhancement of photocurrent can occur if the photoexcited dye transfer carrier into TiO_2 in the first tens of femtosecond before the decoherence of plasmon occurs. In another work of Zarick *et al* [36], plasmonic enhancement of shape controlled ~ 45 nm edge-length Au nano-cubes coated with a 5 nm silica layer, Au@SiO$_2$ nano-cubes has been demonstrated. They observed ~34% improvement in power conversion efficiency. Contrary to the work described by Snaith and co-workers, they attributed the improved device efficiencies by the Au@SiO$_2$ nano-cubes to radiative effects. All together after photoexcitation different plasmonic phenomena in the NPs like electron-electron scattering or electron-phonon scattering happening on very fast time scales, competes with associated energy and charge transfer or light field enhancement due to LSPR, and further understanding of this charge transport kinetics at dye/metal interface with time-resolved spectroscopies is necessary for complete understanding.

Here, in this mini review, we summarize of our investigations on excited state carrier injection dynamics of two thioalkyl substituted tetrathiafulvalene molecules referred to as G1, and G3 as thin film deposited on mesoporous TiO_2 and also demonstrate the effect of plasmonic enhancement due to AgNPs in between dyes and TiO_2 layers [37,38] The DSSC devices employing G1 and G3 molecules exhibited photo-current conversion efficiency of 6.6 and 7.15%, respectively [39]. Further, a complete excited state dynamics of these molecules in solutions and thin-films have been reported in our earlier work [37]. Herein, we performed both linear and time-resolved spectroscopy experiments in thin film of the dyes

deposited on a mesoporous TiO_2 layer as well as incorporating a thin AgNP layer between dye and TiO_2 to elucidate the electron-injection rate at the G1 (and G3)-TiO_2 interface and G1 (and G3)-AgNP-TiO_2 interface and the associated recombination dynamics enlightening the effect of AgNPs. The steady-state PL and the TRPL measurements for dye-TiO_2 samples provided the initial proof of efficient charge injection via observation of enhanced PL quenching. The TAS data further revealed a multi-step electron injection at the interfaces upon photoexcitation of both molecules with the ultrafast injection component to be of ~374 fs and ~314 fs for G1-TiO_2 and G3-TiO_2 samples, respectively. While due to presence of AgNP layer between dye/TiO_2 interface, we observed enhanced photobleaching and hot electron injection from AgNPs to TiO_2 resulting more light absorption bye the sensitizers as well as enhanced carrier injection rate.

2 Experimental Details

2.1 Materials

The structure of the sensitizers considered here, along with their abbreviations (G1 and G3), are shown in Figure 1(a). The two dyes have been designed on tetrathiafulvalene scaffold by implementing a donor-π-acceptor (*D-π-A*) approach in which thioalkyl substituted tetrathiafulvalene acts as a donor, substituted anthracene i.e., either 2-(anthracene-2-yl) thiophene (G1) or 2-(anthracene-2-ylethynyl) thiophene (G3) as a π-spacer and cyanoacrylic acid acts as an acceptor as well as an anchoring group. The detailed synthesis process, spectroscopic, electrochemical and DFT studies of these dyes are reported elsewhere [39]. The molecules were deposited on a quartz substrate using the drop-casting method to prepare thin-film samples. For dye-TiO_2 films, first titania nanoparticle paste (purchased from Sigma-Aldrich) was deposited on properly cleaned quartz substrates using the doctor-blade method and thereafter annealed at for 30 minutes to prepare mesoporous TiO_2 layers. Thereafter, these TiO_2 films are sensitized with the dyes and the sensitized films showed good optical transparency in the visible region and have been used in all spectroscopic studies herein. For 'Dye-Ag nanoparticle-TiO_2' composite thin film, the composite nanoparticle (NP) thin films were prepared by adding a thin layer of fs-laser ablated Ag nanoparticles (~35 nm) between dye and mesoporous TiO_2 layers.

2.2 Photoluminescence measurements

The steady-state photoluminescence (PL) spectra of the dyes in thin-films were obtained using FLS 1000 spectrometer (Edinburgh Instruments). The PL spectra of thin-film samples were collected using a special holder with a inclination angle; thus avoiding increased reflections of the excitation beam toward the detection pathway. Time-resolved photoluminescence (TrPL) measurement was performed using the standard Time-Correlated Single Photon Counting (TCSPC) technique integrated with FLS 1000 using a picosecond diode laser with wavelength 405 nm. The instrument response function (IRF) was recorded by placing plane quartz substrates. Photoluminescence curves were fitted by the re-convolution method using the corresponding IRF to extract the life-time parameters from the whole time-resolved measurement. The quality of the fit was judged by the χ^2 values and distribution of residuals.

2.3 Femtosecond transient absorption measurements

The femtosecond transient absorption (fs-TAS) measurements were performed using a commercial transient absorption spectrometer (HELIOS) based on a Ti: Sapphire regenerative amplifier (LIBRA, M/s Coherent, USA) delivering 1 kHz, ~4 mJ pulses with a central wavelength of 800 nm and pulse duration of ~70 fs (FWHM) at the output. The output pulses were split into two parts. One part was used for white light generation, from 430 nm to 780 nm, after focusing into a 3 mm thick sapphire window. The other fraction was frequency doubled to generate a 400 nm excitation beam. The fluence of the excitation beam at the sample was approximately 0.1 mJ/cm^2, and its polarization was at a magic angle with respect to the probe beam. The film samples were placed in a holder, which was constantly moved randomly, on a

plane perpendicular to the excitation beam. The TA spectra were corrected for the chirp of the white-light probe pulses. To obtain a photophysical description of the excited state evolution in terms of precisely estimated rate constants and evolution and species-related spectral signatures, the transient data reported here were analysed using a combination of global and target analysis. In this work, the TA data of thin-films of dyes are globally analysed using sequential kinetic model, an unbranched and unidirectional model, consisting of successive mono-exponential decays with increasing time constants estimating gross spectral evolution of the data, giving evolution associated difference spectra (EADS). The minimum number of independent components required in the sequential model fitted to all data was determined by the singular value decomposition (SVD) method as well as checking that the residuals were effectively zero. The TA data of dyes deposited on TiO_2 and dye-AgNp-TiO_2 films were fitted through target analysis using a compartmental scheme based kinetic model. This analysis estimates the real spectra of each compartment (excited species) including branching ratios for electron injection manifesting species-associated-difference-spectra (SADS). The whole analysis was performed with the R package TIMP and its graphical user interface, Glotaran 1.5.1 (complete description can be found in literature) [40].
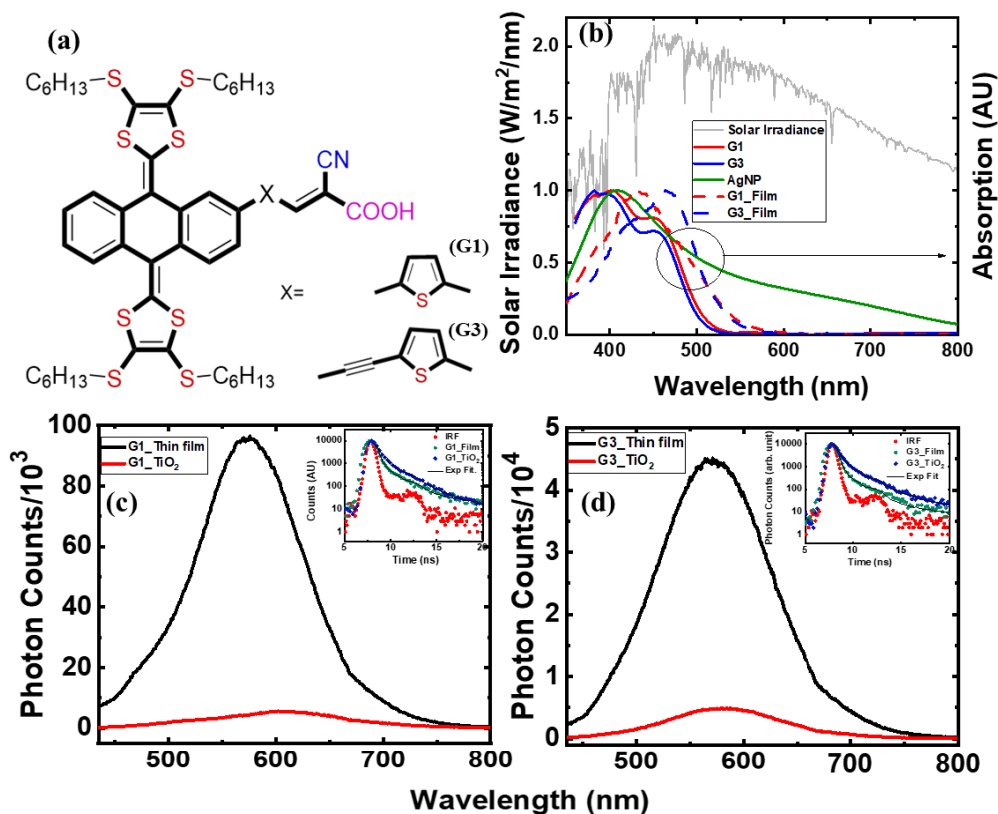
Fig 1. (a) The molecular structures of tetrathiafulvalene based extended π-conjugated sensitizers (G1 and G3); (b) Solar irradiance overlaid with absorption spectra of the sensitizers and Ag NPs. Red and blue solid lines are for G1 and G3 solution dissolved in DMF solvent. Red and blue dash lines are for G1 and G3 films on transparent glass substrates and the green solid line is for Ag NPs; (c) & (d)- comparative measurement of steady-state fluorescence spectra of the dyes on quartz substrate and mesoporous TiO_2 substrate for G1 and G3, respectively, illustrating the quenching of photoluminescence intensity upon TiO_2 surface. Insets show TCSPC lifetime decay curves (at room temperature) of the dyes in 8-20 ns time window for G1 and G3 as thin films deposited on quartz substrate and TiO_2 surface, respectively. Open symbols represent experimental data and solid lines represent multiexponential re-convolution fits using instrument response function (IRF).

3 Results and Discussion

3.1 Absorption and fluorescence measurements

The normalized visible absorption of G1 and G3 sensitizers (red and blue curves, respectively) in the DMF solvent are shown in Fig 1(b). Spectroscopy grade DMF was used to prepare a dilute solution of 10 μM concentration. In the solution, G1 and G3 exhibited absorption maximum at 403 and 397 nm, respectively and for both molecules, shoulder peaks are observed with a maximum at 451 and 452 nm wavelengths, respectively. The green curve in Fig 1(b) is normalized absorption of AgNPs in solution form with absorption maxima around 415 nm, with long tail extending over the entire visible range. For comparison purposes the solar irradiance is also overlaid with the dye and AgNPs absorption. It is clear from the graph that the dyes absorb a broad range of visible spectrum 350 to ~ 530 nm, whereas the AgNPs also have strong absorption in this region along with extended absorption 530 nm to 800 nm, thus incorporation of AgNP in the dye-TiO$_2$ interface will enhance overall light absorption of the active layer. Red and blue dashed lines indicate the absorption of G1 and G3 thin films in quartz substrate, with absorption maximum around wavelengths of 430 and 460 nm, respectively. The steady-state fluorescence spectra of G1 and G3 sensitizers deposited as thin films on a quartz substrate are shown in Fig 1(c) and (d) represented by the black lines. To measure the fluorescence emission, the samples were excited at 400 nm wavelength. The emission peaks of G1 and G3 films are at ~570 and ~576 nm, respectively. For comparative purposes, we have measured the steady-state emission spectra of the sensitizer adsorbed on the mesoporous TiO$_2$ keeping the experimental parameters same. In Figs 1(c) and 1(d) red lines illustrate the absorption corrected emission spectra of G1 and G3 adsorbed on TiO$_2$, clearly showing efficient emission quenching of both the sensitizers on TiO$_2$ indicating electron transfer from the excited dye to the conduction band (CB) of TiO$_2$. The estimated emission quenching for both G1-TiO$_2$ and G3-TiO$_2$ films are ≈90%. This is expected as the LUMO positions of G1 and G3 were estimated to be 2.74 eV and 2.89 eV, respectively [39], which is above the CB of the TiO$_2$ (~ 4.03 eV), thus enabling a favorable electron injection. This results in a reduced population of the excited state to decay to the ground state, thereby manifesting as efficient PL quenching. To shed more light on the quenching process, we have investigated the PL lifetime dynamics. Insets in Figs 1(c) and (d) present the comparison of fluorescence dynamics within a 5-20 ns time scale of G1 and G3 dyes in different environments (in each case for the measurements, the experimental parameters have been maintained identical). Inset in Fig 1(c) compares fluorescence decay of G1 on quartz and TiO$_2$, and it is apparent that when G1 is adsorbed on TiO$_2$ mesoporous layers the recombination reduces slowing down the PL decay compared to G1 deposited on quartz, and this directly indicated population is being injected from dye excited state to CB of TiO$_2$. Similar behavior was observed in Fig 1(d) inset for the G3 dye deposited as a thin film on quartz and mesoporous TiO$_2$ layers.

3.2 Femtosecond transient absorption measurements

Femtosecond transient absorption spectroscopy (TAS) measurements allow us to identify the generation of dye cations formed after injection of electrons from the dye's excited state to the conduction band of the semiconductor and the corresponding TA spectra can contain overlapping contributions from other species such as excited molecules and/or injected electrons. Therefore, ultrafast transient absorption measurements of the sensitizers G1 and G3 thin films, adsorbed on TiO$_2$ layer and incorporated with AgNP in dye-TiO$_2$ layer were performed to provide a complete understanding of the electron injection and charge recombination mechanism.

To investigate the electron injection process from dye to TiO$_2$, we measured the TA spectra of G1 and G3 adsorbed on the mesoporous TiO$_2$ layer deposited on quartz substrate with excitation at 400 nm. Figures 2 (a & b) present the selected TA spectra at different probe delays starting from 300 fs to 2 ns measured for G1 and G3 adsorbed on TiO$_2$, respectively. To distinguish the effect of electron injection from

dye to TiO$_2$ on dye-TiO$_2$ transient data, we have also measured TA spectra of only dye thin film on bare quartz substrate, where there are no possibilities of charge injection. The insets in Fig 2(a & b) represents TA spectra of G1 and G3 bare thin film within probe delays 300 fs to 2 ns. From the TA data of bare thin films, it was observed that the obtained spectra for G1 film (inset in Fig 2(a)) have two distinct regions: (i) spectral region 486-546 nm demostrating a negative band which represents the ground state-state bleach (GSB), and (ii) spectral region 545-780 nm demonstrating a broad positive band which represents a photoinduced absorption (PIA) with a peak around 693 nm. Similarly, two distinct regions are also observed in the TA spectra of G3 in the inset of Fig 2(b). For the case of G3, the ESA band shows a red shift of ~30 nm with
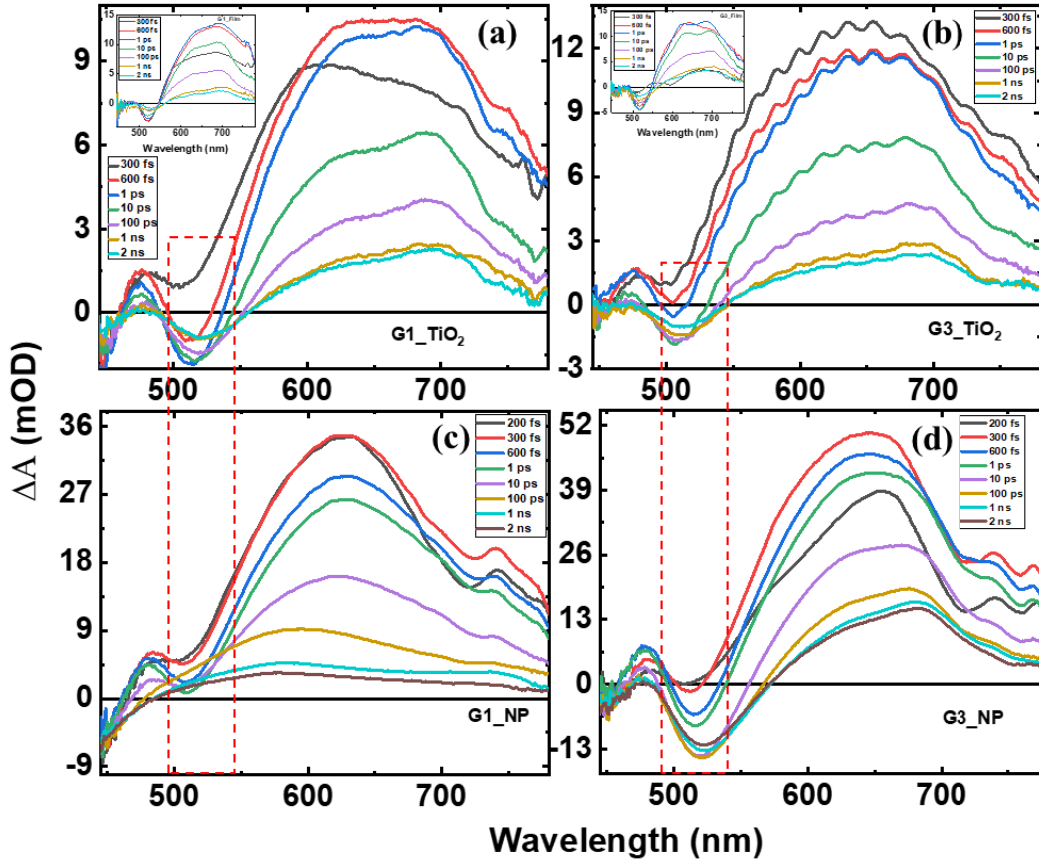
Fig 2. Temporal evolution of individual experimental transient absorption spectra (ΔA in mOD): (a)-for 'Dye (G1)-TiO$_2$' composite thin film, the inset showing spectra for Dye (G1) only film; (b)-for 'Dye (G3)-TiO$_2$' composite thin film and the inset represents ΔA spectra for Dye (G3) only film; (c) and (d)- for 'Dye (G1)-Ag nanoparticle-TiO$_2$' and 'Dye (G3)-Ag nanoparticle-TiO$_2$' composite thin films, respectively. For all ΔA measurements pump wavelength was 400 nm. The red dashed box highlights the photo bleach band for both kind of films.

the evolution of time from 300 fs to 2 ns. From the temporal evolution of the GSB band for G1, it was observed that the intensity of bleach decreases starting from 300 fs to 2 ns, whereas for G3 the GSB intensity initially increases from 300 to 10 ps and then decreases up to 2 ns. For the ESA band, the temporal evolution revealed that for both the dyes the intensity of the ESA band initially increases (from 300 fs to 1 ps spectra) and then decreases (up to 2 ns spectra). Whereas, for dye-TiO$_2$ films (Fig 2(a) and (b)) a new positive band is observed at about < 300 fs after excitation in the spectral window of 450 - 495 nm for both the dyes.

This band coincides with the dye cation absorption as confirmed by the spectro electrochemical absorption measurements with controlled potential oxidation of the dye molecules shown in the previous reports [37]. This suggests the ultrafast formation of the dye cation in the dye/TiO$_2$ film upon electron injection into the conduction band of TiO$_2$. Importantly there is no spectral signature in this spectral region for the TAS measurements for G1 and G3 thin films on quartz (insets of Fig 2(a & b)) as there is no possibility of electron injection. In its excited state, the donor-π-acceptor structure of the dyes induces intramolecular charge transfer (ICT) from the tetrathiafulvalene unit (donor) to the cyanoacrylic unit (acceptor) such that the electron cloud localizes on cyanoacrylic unit in the LUMO level [39]. Therefore, upon sensitization of the TiO$_2$ with the dye where the cyanoacrylic group anchors with TiO$_2$ atoms available on the surface of TiO$_2$, the formation of ICT favors efficient charge transfer from the excited state (i.e., higher singlet states (S_n)) as well as relaxed intermediate states to the CB of TiO$_2$ via the anchor unit of the dye molecule. It is also observed that GSB recovery is very slow (> 4 ns) and ESA exhibits a large shift towards longer wavelengths with increasing time compared to the thin film TA spectra, indicating the difference in the excited state process compared to the dye thin films on the quartz substrates.

To investigate the plasmonic enhancement in photo absorption and electron injection of the dyes, in presence of Ag nanoparticles, TA spectra of 'Dye-Ag nanoparticle-TiO$_2$' composite thin film' Figs 2(c) and 2(d) represent the fs-TA spectra at selected probe delays starting from 200 fs to 2 ns for the composite films with G1 and G3, respectively. The composite nanoparticle (NP) thin films were prepared by adding a thin layer of laser ablated Ag nanoparticles (~35 nm) between dye and mesoporous TiO$_2$ layers. For dye G1, from Fig 2(c) it is observed that due to incorporation of Ag-nanoparticle the GSB band is strongly overlapped with the ESA band compared to Dye(G1)-TiO$_2$ film. Whereas, for G3 from Fig 2(d) it is observed that the photo-bleaching signal is enhanced in intensity and is red shifted by 13 nm due to presence of Ag nanoparticle compared to Dye(G3)-TiO$_2$ film, indicating plasmonic enhancement of the photo absorption of dye molecules. Due to the strong spectral overlap between AgNPs and G1 and G3 dyes, the observed photobleaching band has contribution from both the photobleaching of the dye and relaxation of plasmons. Also, the excitation power is same for both kind of samples, suggesting that the presence of Ag nanoparticle has increased the dye photobleaching signal and thus enhanced the charge generation.

3.3 Global and target analysis

Due to the overlapping nature of the spectral signatures, it is difficult to analyze and interpret the TA dynamics by the single wavelength-kinetic fitting. Therefore, the TA data matrix is analyzed using singular value decomposition (SVD) to find out the minimum principal components required to fit the entire data matrix. And then based on this number of principal kinetics global and target analysis of the data has been done to precisely estimate rate constants and species related spectral signature. For the case of G1 & G3 thin films on quartz, no charge injection process is expected, and after the photoexcitation, all the population eventually reach the ground state sequentially. For the case of dye-TiO$_2$, and dye-AgNPs-TiO$_2$ population transfer occurs due to the electron injection to CB of the TiO$_2$ or into the trap states or hot electron injection from NPs at the interface with the concomitant formation of cation species. Therefore, target analysis is used to consider all the plausible processes that occur in the dye-TiO$_2$ or dye-AgNPs-TiO$_2$ interface. The target analysis used compartmental based kinetic model, considering all possible branching of population (electron-injection) from dye excited state to conduction band of TiO$_2$ and Ag nanoparticle charge transfer states. For dye-TiO$_2$ interface, at least four compartments were required to obtain a satisfactory description of the data, and the best possible model accordingly is presented in Fig 3. The associated rate constants and lifetimes of excited states for dye-TiO$_2$ and dye-AgNP-TiO$_2$ samples are recorded in Table 1. Following photoexcitation, at 400 nm the population excite to singlet S_n state. From S_n state two parallel decay pathways are taking place i.e., from $S_n - S_1^*$ via internal conversion and $S_n - $ TiO$_2$ CB via electron transfer. From S_1^* some of

the population relaxes to S_1 via vibrational relaxation and some part is being injected to TiO_2 CB. From S_1, there are possible branching of the decay channel for the population to be transferred to TiO_2 CB. Finally, ground state S_0 is recovered by radiative decay from S_1 and charge recombination from the lower-lying trap states from the interface of TiO_2 CB. It should be noted that the extraction of the trustworthy value of recombination rate from TiO_2 CB, i.e., k_{40}, from TA data of 2ns time window is unrealistic. Therefore, k_{40} was kept as a constraint to fit to be greater than 2ns. Based on this target-scheme, obtained experimental TA spectral data are reproduced well and the spectra along with lifetimes of the compartments/states and related rate constants are estimated.
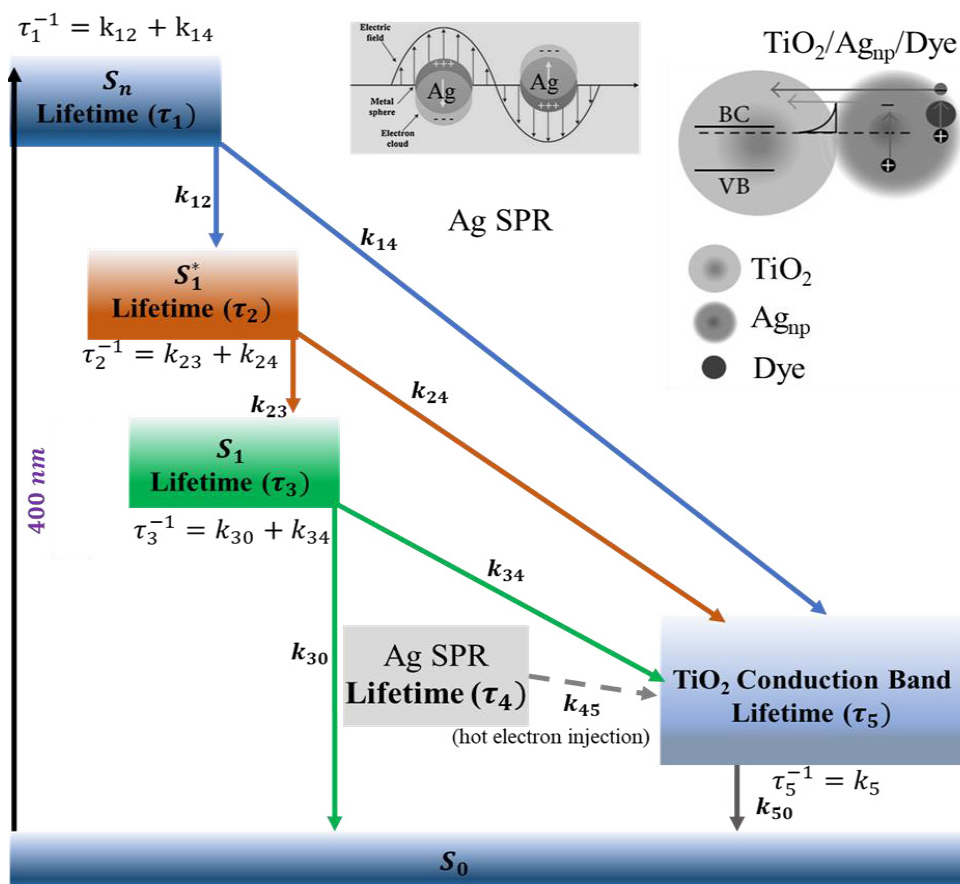
Fig 3. Schematic diagram of the photophysical kinetic model used for target analysis of TA data for 'Dye-TiO₂' composite film as well as 'Dye-Ag nanoparticle-TiO₂' film (for this case the gray scale channel is considered).

While for 'Dye-Ag nanoparticle-TiO₂' SVD analysis predicted at least 5 compartments to describe the TAS data as shown in Fig 3, where the hot electron injection channel is introduced. Figure 4 (a) and (b) illustrate the obtained species associated difference spectra (SADS) from target analysis of NP composite films, and from SADS it was observed that the kinetic model well reproduced the experimental data. Target analysis of 'Dye-TiO₂' films revealed ultrafast electron injection times of ~374 fs and ~314 fs for G1 and G3 molecules, respectively along with two slow components with lifetimes 1.01 ps (2.54 ps) and 74.65 ps (111.29 ps) for G3 (G1) molecules. From the analysis, upon incorporating Ag nanoparticles, it was found that

(Table 1) for 'G1-Ag nanoparticle-TiO_2' composite, the entire spectra can be reproduced from 5 principal species with lifetimes: (578 fs & 343 fs), (3.07 ps & 2.42 ps), (153.14 ps, 109.89 ps), 281 ps and 8340 ns. For 'G3-Ag nanoparticle-TiO_2' composite, these lifetimes are (0.662 fs & 0.305 fs), (1.60 ps & 1.03 ps), (138.12 ps & 64.02 ps), 286 ps, and 8340 ps. In the case of 'Dye-Ag nanoparticle-TiO_2' films for transition the first lifetimes (Table 1) are 343 fs for G1 and 305 fs for G3. It is evident that upon incorporation of Ag nanoparticles electron injection from dye to TiO_2 is more efficient. Also, we found that the hot electron injection from AgNp to TiO_2 is happening within ~280 ps. Figures 4(c) and 4(d) compare the representative TA decay profiles of 'Dye (G1 and G3, respectively)-Ag nanoparticle-TiO_2' composite thin film and 'Dye (G1 and G3, respectively)-TiO_2' composite thin film. Open scattered symbols are experimental data and solid lines are fits obtained from target analysis. From the comparison, it is observed that kinetics corresponding to cation band (480 nm) and GSB band (510 nm) decay slowly for NP composite films compared to dye TiO_2 films indicating better population transfer and reduced charge recombination. indicating better population transfer and reduced charge recombination.
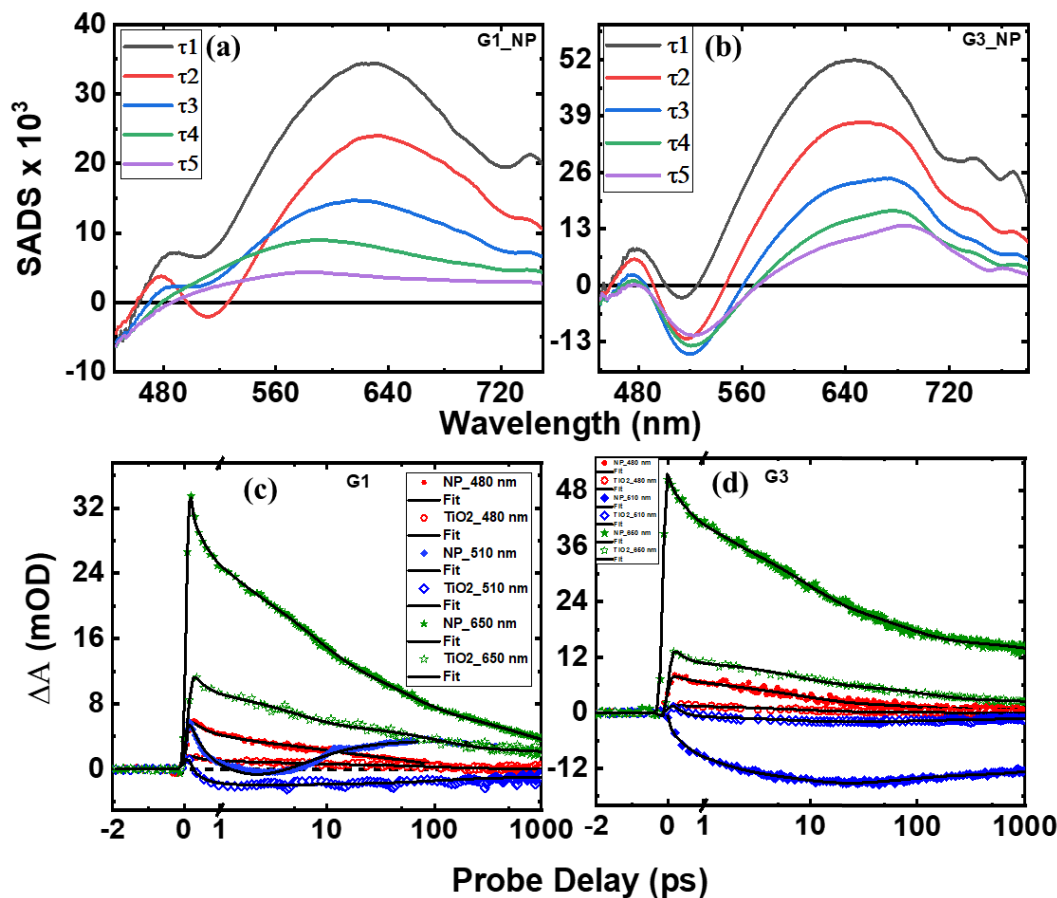
Fig 4. (a) and (b). Species-associated difference spectra (SADS) for TA data of Dye (G1 and G3, respectively)-Ag nanoparticles-TiO_2 composite thin films resulting from target analysis; (c) and (d)- comparison of representative TA decay profiles (at ~ 480 nm in cation band, 510 nm in GSB-, and 650 nm in ESA- band) between 'Dye (G1 and G3, respectively)-Ag nanoparticle-TiO_2' composite film and 'Dye (G1 and G3, respectively)-TiO_2' composite film. Open scattered symbols are experimental data and solid lines are fits obtained from global analysis.

Table 1. Lifetimes and rate constants obtained from global and target analysis of TA data of G1(G3) deposited on TiO_2 and "G1(G3)-Ag nanoparticle-TiO_2" composite thin films.

Rate constants ($\times 10^{12}$ ps^{-1})				Time constants (*in ps*)				Electron injection times			
G1_TiO_2	G1_ Ag$_{np}$_ TiO_2	G3_TiO_2	G3_ Ag$_{np}$_ TiO_2	G1_TiO_2	G1_ Ag$_{np}$_ TiO_2	G3_TiO_2	G3_ Ag$_{np}$_ TiO_2	G1_TiO_2	G1_ Ag$_{np}$_ TiO_2	G3_TiO_2	G3_ Ag$_{np}$_ TiO_2
$k_{12} = 1.44$ $k_{14} = 2.67$	1.73 2.91	$k_{12} = 1.43$ $k_{14} = 3.18$	1.51 3.27	$\tau_{12} = 0.694$ $\tau_{14} = 0.374$	0.578 0.343	$\tau_{12} = 0.700$ $\tau_{14} = 0.314$	0.662 0.305	τ_{et} (S_n–CB) = 374 fs	τ_{et} (S_n–CB) =343 fs	τ_{et} (S_n–CB) =314 fs	τ_{et} (S_n–CB) =305 fs
$k_{23} = 0.29670$ $k_{24} = 0.39371$	0.32561 0.41256	$k_{23} = 0.55252$ $k_{24} = 0.99001$	0.62456 0.97451	$\tau_{23} = 3.37$ $\tau_{24} = 2.54$	3.07 2.42	$\tau_{23} = 1.81$ $\tau_{24} = 1.01$	1.60 1.03	τ_{et} (S_1^*–CB) = 2.54 ps	τ_{et} (S_1^*–CB) = 2.42 *ps*	τ_{et} (S_1^*–CB) = 1.01 *ps*	τ_{et} (S_1^*–CB) = 1.03 *ps*
$k_{30} = 0.00551$ $k_{34} = 0.00890$	0.00653 0.00910	$k_{30} = 0.00547$ $k_{34} = 0.01339$	0.00724 0.01562	$\tau_{30} = 181.58$ $\tau_{34} = 111.29$	153.14 109.89	$\tau_{30} = 182.76$ $\tau_{34} = 74.65$	138.12 64.02	τ_{et} (S_1–CB) = 111.29 ps	τ_{et} (S_1–CB) = 109.89 *ps*	τ_{et} (S_1–CB) = 74.65 ps	τ_{et} (S_1–CB) = 64.02 *ps*
$k_4 = 0.00015$	3.56	$k_4 = 0.000145$	3.49	$\tau_4 = 6590$	0.281	$\tau_4 = 6890$	0.286		τ_{et} (Agspr-CB) = 281 fs		τ_{et} (Agspr-CB) = 286 fs
	$k_5 \sim$ 0.00012		$k_5 \sim$ 0.00012		τ_5 ~8340	τ_5 ~8340					

4 Conclusions

In summary, this mini-review provides a brief description of the role of ultrafast electron injection at the dye-TiO_2 interface for efficient dye sensitized solar cell devices and present the ultrafast charge-injection dynamics of two novel D–π–A organic sensitizers (G1 and G3) using a combination of steady-state, time-resolved photoluminescence, and femtosecond transient absorption spectroscopy in the visible regions. Time-resolved photoluminescence and transient absorption measurements on TiO_2 have shown an ultrafast electron injection for both the dyes. The obtained data showed ultrafast injection times of ~374 fs and ~314 fs for G1 and G3 molecules, respectively along with two slow components with lifetimes 1.01 ps (2.54 ps) and 74.65 ps (111.29 ps) for G3 (G1) molecules thus proving the better DSSC device efficiency with G3 molecule compared to that of G1 in agreement with the previous study. Furthermore, we have also reviewed the plasmonic enhancement of light harvesting properties of G1 and G3 incorporating silver (Ag) nanoparticles deposited as a thin layer between dye and mesoporous TiO_2 layers, using transient absorption spectroscopy. We have observed more efficient charge injection into TiO_2 conduction band from dye excited state and reduced back recombination of charges in the presence of AgNPs in the dye-TiO_2 interface.

References

1. Hardin B E, Snaith H J, McGehee M D, The renaissance of dye-sensitized solar cells, *Nat Photonics*, 6(2012)162–169.
2. Hagfeldt A, Boschloo G, Sun L, Kloo L, Pettersson H, Dye-sensitized solar cells, *Chem Rev*, 110(2010)6595-6663.
3. Mishra A, Fischer M K, Bäuerle P, Metal-free organic dyes for dye-sensitized solar cells: From structure: Property relationships to design rules, *Angew Chem Int*, 48(2009)2474–2499.
4. Listorti A, O'regan B, Durrant J R, Electron transfer dynamics in dye-sensitized solar cells, *Chemi Mater*, 23(2011)3381-3399.
5. Chen Z, Li F, Huang C, Organic D-π-A dyes for dye-sensitized solar cell, *Curr Org Chem*, 11(2007)1241-1258.
6. Bairu S G, Mghanga E, Hasan J, Kola S, Rao V J, Bhanuprakash K, Giribabu L, Wiederrecht G P, da Silva R, Rego L G, Ultrafast interfacial charge-transfer dynamics in a donor-π-acceptor chromophore sensitized TiO_2 nanocomposite, *J Phys Chem C*, 117(2013)4824-4835.
7. Kakiage K, Aoyama Y, Yano T, Oya K, Fujisawa J-I, Hanaya M, Highly-efficient dye-sensitized solar cells with collaborative sensitization by silyl-anchor and carboxy-anchor dyes, *Chem Commun*, 51(2015)15894–15897.
8. Wang P, Zakeeruddin S M, Moser J E, Nazeeruddin M K, Sekiguchi T, Grätzel M, A stable quasi-solid-state dye-sensitized solar cell with an amphiphilic ruthenium sensitizer and polymer gel electrolyte, *Nat Mater*, 2(2003)402-407.
9. Nazeeruddin M K, Bessho T, Cevey L, Ito S, Klein C, Angelis F D, Fantacci S, Comte P, Liska P, Imai H, A high molar extinction coefficient charge transfer sensitizer and its application in dye-sensitized solar cell, *J Photochem Photobiol A: Chem*, 185(2007)331–337.
10. Grätzel M, Recent advances in sensitized mesoscopic solar cells, *Acc Chem Res*, 42(2009)1788–1798.
11. Mora-Seró I, Bisquert J, Breakthroughs in the development of semiconductor-sensitized solar cells, *J Phys Chem Lett*, 1(2010)3046-3052.
12. Sambur J B, Novet T, Parkinson B, Multiple exciton collection in a sensitized photovoltaic system, *Science*, 330(2010)63–66.
13. Law M, Greene L E, Johnson J C, Saykally R, Yang P, Nanowire dye-sensitized solar cells, *Nat Mater*, 4(2005)455–459.
14. Villanueva-Cab J, Jang S.-R, Halverson A F, Zhu K, Frank A J, Trap-free transport in ordered and disordered TiO_2 nanostructures, *Nano Lett*, 14(2014)2305–2309.
15. Yella Y, Lee H.-W, Tsao H N, Yi C, Chandiran A K, Nazeeruddin M K, Diau E W.-G, Yeh C.-Y, Zakeeruddin S M, Grätzel M, Porphyrin-sensitized solar cells with cobalt (II/III)–based redox electrolyte exceed 12 percent efficiency, *Science*, 334(2011)629–634.
16. Green M A, Pillai S, Harnessing plasmonics for solar cells, *Nat Photonics*, 6(2012)130–132.
17. Polman A, Atwater H A, Photonic design principles for ultrahigh-efficiency photovoltaics. *Nat Mater*, 11(2012)174–177.
18. Atwater H A, Polman A, Plasmonics for improved photovoltaic devices, In Materials for sustainable energy: A collection of peer-reviewed research and review articles from nature publishing group, 2011: p. 1-11.
19. Erwin W R, Zarick H F, Talbert E M, Bardhan R, Light trapping in mesoporous solar cells with plasmonic nanostructures, *Energy Environ Sci*, 9(2016)1577–1601.
20. Atwater H A, Polman A, Plasmonics for Improved Photovoltaic Devices, *Nat Mater*, 9(2010)205–213.
21. Ramakrishna S, Pelton M, Gray S K, Seideman T, Plasmon-enhanced electron injection in dye-sensitized solar cells, *J Phys Chem C*, 119(2015)22640–22645.
22. Brown M D, Brown, Suteewong T, Kumar R S S, D'Innocenzo V, Petrozza A, Lee M M, Wiesner U, Snaith H J, Plasmonic dye-sensitized solar cells using core− shell metal− insulator nanoparticles, *Nano Lett*, 11(2011)438–445.
23. Ihara M, Kanno M, Inoue S, Photoabsorption-enhanced dye-sensitized solar cell by using localized surface plasmon of silver nanoparticles modified with polymer, *Physica E: Low Dimens Syst Nanostruct*, 42(2010)2867–2871.
24. Knight M W, Sobhani H, Nordlander P, Halas N J, Photodetection with active optical antennas, *Science*, 332(2011)702–704.
25. Li J, Cushing S K, Meng F, Senty T R, Bristow A D, Wu N, Plasmon-induced resonance energy transfer for solar energy conversion, *Nat Photonics*, 9(2015)601–607.

26. Grätzel M, Photoelectrochemical cells, in Materials For Sustainable Energy: A Collection of Peer-Reviewed Research and Review Articles from Nature Publishing Group, (World Scientific), pp 26-32.

27. Ren X, Jiang S, Cha M, Zhou G, Wang Z.-S, Thiophene-bridged double D-π-A dye for efficient dye-sensitized solar cell, *Chem Mater*, 24(2012)3493-3499.

28. Martín C, Ziółek M, Marchena M, Douhal A, Interfacial Electron Transfer Dynamics in a Solar Cell Organic Dye Anchored to Semiconductor Particle and Aluminum-Doped Mesoporous Materials, *J Phys Chem C*, 115(2011)23183-23191.

29. Gil M, Ziółek M, Organero J A, Douhal A, Confined fast and ultrafast dynamics of a photochromic proton-transfer within a zeolite nanocage, *J Phys Chem C*, 114(2010)9554–9562.

30. Hoff D A, Silva R da, Rego L G, Coupled electron–hole quantum dynamics on D− π–A dye-sensitized TiO_2 semiconductors. *J Phys Chem C*, 116(2012)21169–21178.

31. Anderson N A, Lian T, Ultrafast electron transfer at the molecule-semiconductor nanoparticle interface, *Annu Rev Phys Chem*, 56(2005)491–519.

32. Duncan W R, Prezhdo O V, Theoretical studies of photoinduced electron transfer in dye-sensitized TiO_2, *Annu Rev Phys Chem*, 58(2007)143-–184.

33. Rego L G, Batista V S, Quantum dynamics simulations of interfacial electron transfer in sensitized TiO_2 semiconductors, *J Am Chem Soc*, 125(2003)7989–7997.

34. Ziółek M, Cohen B, Yang X, Sun L, Paulose M, Varghese O K, Grimes C A, Douhal A, Femtosecond to millisecond studies of electron transfer processes in a donor–(π-spacer)–acceptor series of organic dyes for solar cells interacting with titania nanoparticles and ordered nanotube array films, *Phys Chem Chem Phys*, 14(2012)2816–2831.

35. Fakis M, Stathatos E, Tsigaridas G, Giannetas V, Persephonis P, Femtosecond decay and electron transfer dynamics of the organic sensitizer D149 and photovoltaic performance in quasi-solid-state dye-sensitized solar cells, *J Phys Chem C*, 115(2011)13429–13437.

36. Zarick H F, Zarick H F, Erwin W R, Boulesbaa A, Hurd O K, Webb J A, Puretzky A A, Geohegan D B, Bardhan R, Improving light harvesting in dye-sensitized solar cells using hybrid bimetallic nanostructures, *ACS Photonics*, 3(2016)385–394.

37. Biswas C, Katturi K N, Duvva N, Giribabu L, Rao S V, Raavi S S K, *Multistep Electron Injection Dynamics and Optical Nonlinearity Investigations of π-Extended Thioalkyl-Substituted Tetrathiafulvalene Sensitizers. J Phys Chem C*, 124(2020)24039–24051.

38. Biswas C, Katturi K N, Duvva N, Giribabu L,Rao S V, Raavi S S K, Plasmon Induced Ultrafast Excited State Interfacial Electron Dynamics of Tetrathiafulvalene Sensitizers. in The 22nd International Conference on Ultrafast Phenomena 2020, OSA Technical Digest (Optical Society of America, 2020), paper M4A.32.

39. Giribabu L, Duvva N, Singh S P, Han L, Bedja I M, Gupta R K, Islam A, Stable and charge recombination minimized π-extended thioalkyl substituted tetrathiafulvalene dye-sensitized solar cells, *Mater Chem Front*, 1 (2017)460–467.

40. Snellenburg J J, Laptenok S P, Seger R, Mullen K M, van Stokkum I H M, Glotaran: A Java-Based Graphical User Interface for the R Package TIMP, *J Stat Soft*, 49(2012) 1-22.

Chinmoy Biswas is currently a Ph D student working with Dr Sai Santosh Kumar Raavi at the Department of Physics, IIT Hyderabad, India. He received M Tech in solid state technology in 2016 from Department of Physics IIT Kharagpur

and M Sc in physics in 2014 from University of Kalyani, West Bengal. His current research interest lies in understanding ultrafast photoinduced process in organic and hybrid perovskite molecules employing mainly femtosecond transient absorption measurements.

Md Soif Ahmed is a Ph D student in the Department of Physics at Indian Institute of Technology Hyderabad. He received his integrated M Sc in Physics from Aliah University, Kolkata in 2017. His current research is focused on excited-state dynamics of functional organic molecules and ultrafast non-linear optics.

Dr Sai Santosh Kumar Raavi is currently an Associate Professor at the Department of Physics, Indian Institute of Technology Hyderabad, India. He received his Ph D from University of Hyderabad in 2009 under the supervision of Prof D Narayana Rao. His main research focus is to work in the area of advanced optical spectroscopy for various functional materials characterization and providing the critical inputs to aid in the fabrication and optimization of energy conversion devices using these materials. He is a senior member of the Optica (Formerly Optical Society of America). He was awarded the FAPESP fellowship to visit IFS-USP, Brazil in 2017 and the Bhaskara Advanced Solar Energy (BASE) fellowship to visit Princeton University in 2019. He has authored and co-authored more than 70 peer-reviewed articles, one book, and two book chapters.